Novel, Low-cost Technique to Manufacture Submillimeter Corrugated Feedhorns

J.M. Munier [*1], A. Maestrini [2], M. Salez [1], M. Guillon [1], and B.Marchand [1].

[1] Laboratoire de Radioastronomie Millimétrique, Observatoire de Paris,
61, avenue de l'Observatoire, 75014 Paris, France.
[2] Submillimeter Wave Advanced Technology group, Jet Propulsion Laboratory,
4800 Oak Grove Drive, Pasadena, CA 91109-8099. Mail Stop 168-314.

ABSTRACT

Corrugated feedhorns are commonly used with reflector antennas, either for emission or reception purposes, because of their very low side lobe beam patterns, their very good E-H plane symmetry and their important bandwidth. Unfortunately, the electroforming technique that is generally used to fabricate them requires the machining of a single-use mandrel. Direct milling of the horn is also possible, either in a single block or in a split block, but this also requires to machine each desired horn. At submillimeter frequencies, machining of small corrugations in a mandrel or in a block is costly. We present in this paper a cost-effective technique to fabricate helicoidal corrugated feed horns, which consists in machining one reusable mandrel and to mold as many horns as needed.

Keywords: Microwave, Millimeter-wave, Submillimeter-wave, Radioastronomy, Radiometers, Corrugated Feedhorns, Antennas, Electroforming, Radio-interferometry, Millimeter arrays.

1. INTRODUCTION

Corrugated horns are often employed because of their low-level sidelobe beam patterns, low return loss, E-H plane symmetry, zero cross-polarization and large bandwidth [1]. These are very attractive criteria for prime-focus feeds or feeds illuminating microwave antennas, in particular in millimeter-wave and submillimeter-wave radiometer applications. Depending on their specific use, their design will range from plain conical shapes and uniform $\lambda/4$ corrugations, to more complex 'profiled' shapes and corrugations of varying depths and width-to-pitch ratios.

Usually, corrugated horns are made out of copper using an electroforming process, the variants of which have been published by several authors [2]. Firstly an aluminum mandrel is machined so as to become the 'negative' of the horn, complete with its waveguide transition and corrugations. Next is the coating of the mandrel with copper by electrodeposition, until the copper body is thick enough to perfectly fill the corrugations and be later resurfaced. As a third step, the aluminum is dissolved in a KOH solution.

Although this manufacture process has reached maturity, it has several drawbacks. The electrodeposition of copper is long (typical rate is 1 mm per week) and a single project may monopolize the manufacturer's equipments for months. Uniform coating of submillimetric size corrugations is difficult. Bubbles in the corrugations are difficult to eliminate due to capillarity effects, and another well-known problem is the formation of voids filled with electrolyte solution due to the faster copper deposition rate at the top than at the bottom of the corrugations. Also, the complete dissolution of aluminum in KOH In addition, fabricating horns by this technique is very costly, since every single horn needs one expensive mandrel to be fabricated and destroyed.

We propose to make corrugated horns differently. By making the corrugations helicoidal and by molding the horn around its negative mandrel, we can reuse the same mandrel as many times as needed to mold new, perfectly identical horns. Although this technique will not be adapted to some of the most complicated corrugation profiles, it will be suited to the design of most corrugated horn practical applications. Not only is the horn fabrication now much faster than using electrodeposition, but the cost will also dramatically decrease when the number of horn units to be made is large.

2. HELICOIDAL HORNS

2.1. Concept.

Depending on the application for which it is designed, a corrugated horn may have the following separate sections playing different roles : a rectangular to circular waveguide transition converting the TE_{10} rectangular waveguide mode into a TE_{11} mode in the circular section ; the so-called 'throat' or matching section which launches spherical wave HE_{11} modes and can be optimized for low standing wave ratio (VSWR) ; the main body of the horn, specified by its aperture and 'flare' angle, which couples the energy into free-space according to a specific diffraction-like beam pattern. The shapes and corrugation profiles of horns may be fairly complex in order to satisfy particular specifications. Because of their simplicity, however, conical corrugated horns are the most commonly employed feeds. One often distinguishes between the 'small' (5°-15°) and 'large' (15°-80°) semi-flare angles, the latter type having a phase center closer to the throat and wider bandwidths [3].

In these novel feedhorns we have replaced the conventional circular corrugated grooves by one or more helicoidal threads spiraling downward from the horn aperture to the start of the throat. The threads have the same rectangular cross-section and spacing as the conventional corrugations (see Fig. 1). Any horn size, flare angle, and even pitch-to-width ratio are allowed. The corrugation depth can be varied along the z-axis as is done in the matching section of most corrugated horns. However, there is a strict rule that both the width and pitch of the corrugation thread be constant. Should this not be done, removing the mandrel would be impossible. It is important to stress that this condition is independent on the horn profile and that, although we shall here focus on conical horns, our process does not rule out more sophisticated horn profiles.

We see that the only main difference between the classical conical design and its proposed helicoidal equivalent resides in that the matching section cannot be optimized for VSWR, since it would require a variation of the corrugation pitch-to-width ratio in the throat. We expected this lack of optimization to be responsible for some

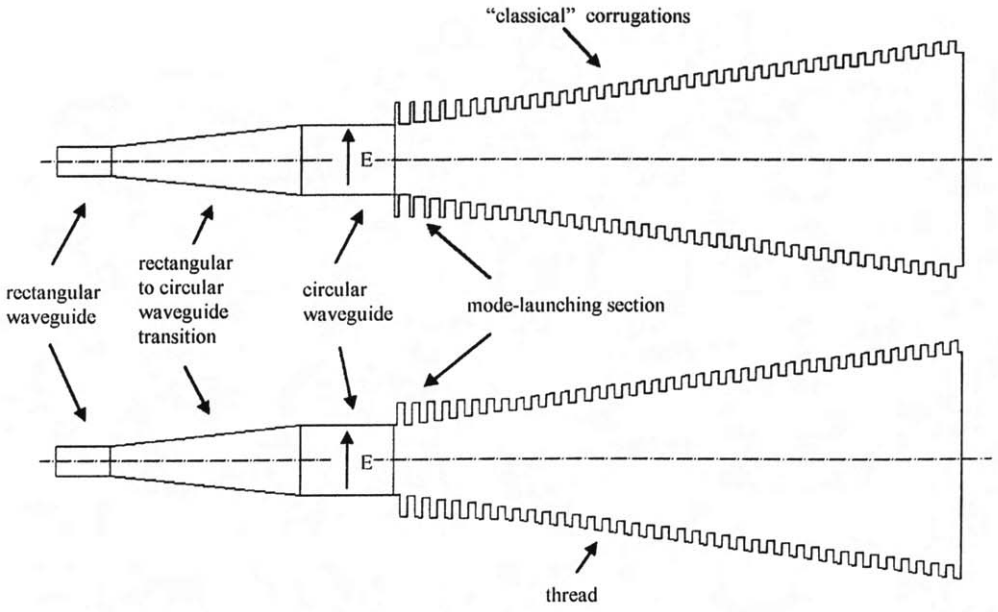

degradation of the S_{11} parameter, and this has indeed been measured.

Fig. 1. Schematics of a classical corrugated horn (top) and its helicoidal equivalent (bottom).

2.2. Fabrication.

The helicoidally corrugated mandrel is machined classically using a milling tour, out of aluminum or rhodium-coated brass. Various numbers of threads can be made. However three is probably a maximum because of the increasing mechanical stress put on the cutting tool by too large a pitch angle. The material we used for the horn is a 'Roses alloy' ($Bi_{50}Pb_{28}Sn_{22}$), chosen for its conveniency and low melting point temperature of 105 °C. Other molding alloy materials could be considered, such as AlMg. The molding is performed in a specially designed housing structure, placing the mandrel under vacuum and letting in the melted alloy under pressure. Once the alloy is solidified, the mandrel is 'unscrewed'. The adherence between the aluminum and the Roses alloy is not sufficiently low to make this operation immediate. It is necessary to put both mandrel and mold in liquid nitrogen, then to warm up only the mold and finally to rotate the mandrel. With this technique, the mandrel offers no resistance when unscrewing. The alloy can be machined afterwards for resurfacing the horn flange and external volume. To reduce the RF losses, the horn can be copper-plated and then gold-plated; but if used in 4 K cryogenic systems, the horn can probably be left without any plating, since the Roses alloy is superconducting at about 6.7 K. Figure 2 shows an early and imperfect prototype of single-thread horn ripped open for examination.

Once the mandrel is available, the operation of molding it with the Roses alloy to obtain a helicoidal horn does not exceed a few hours, including preparation. This is to oppose to weeks of uninterrupted copper electrodeposition in the current process. Each new horn replica only requires the same small amount of time since the mandrel is reused. Should there be a need for large numbers of identical horns to be fabricated, this novel process is well suited for some kind of industrial automation. As for any replication process after a 'master', a very high level of reproducibility would be reached.

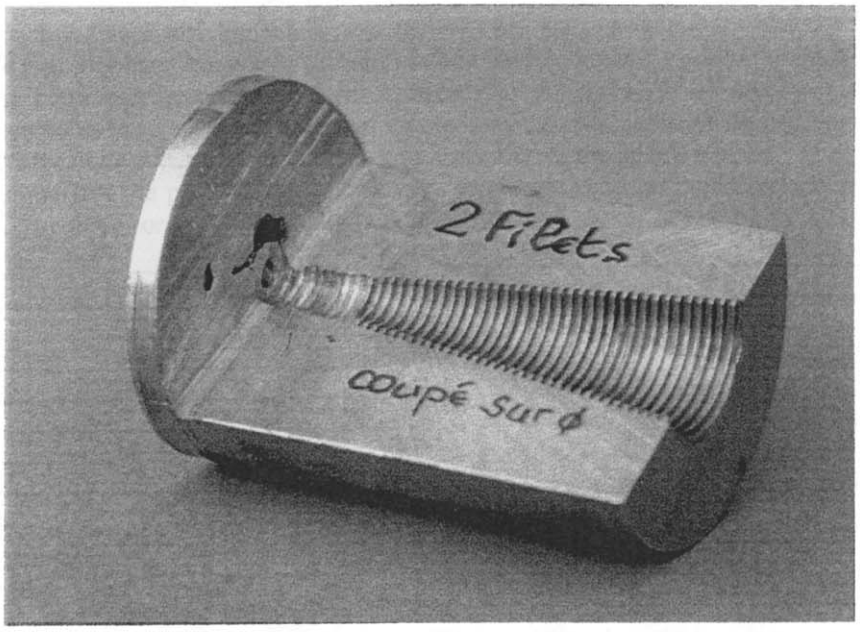

Fig. 2. Photograph of a 110 GHz single-thread helicoidal horn prototype sacrificed for examination, showing the corrugations quality. A few corrugations near the throat are missing due to a defect having occurred during molding.

3. CHARACTERIZATION AT 100 - 120 GHz

3.1. Helicoidal horns for 110 GHz.

We chose to demonstrate the technology on small flare angle horns, since they are the most constraining from the standpoint of this novel manufacturing process. In order to validate the practical use of the helicoidal horn concept, it was important to make comparative measurements fo their performance with a reference horn. We have thus based the design of our test horns on a high-quality horn at 110 GHz available in the lab and initially designed for a *Meteosat* development [4]. It must be noted that this choice of frequency to validate the process was also driven by a

need for high dynamics measurements. Yet there is no fundamental difficulty in extending the helicoidal concept to frequencies much higher (needless to say, lower) than 110 GHz.

Obviously, the new important parameter of the novel design is the pitch, or slant angle of the threads. While this angle is evidently 0 for all classical horns, it is now $\neq 0$ and varies along the z-axis and depending upon how many threads one wishes to squeeze in the horn. If p is the pitch of a classical horn and of its single-thread equivalent, then the pitch of the helicoidal horn with N threads will be $N.p$. For practical reasons, we limited ourselves to three horns labelled 'A', 'B' and 'C' having the exact same size, flare angle and corrugation profile, but with respectively one, two and three threads. Therefore horn C is the most difficult to fabricate because it has corrugated grooves three times more slanted than horn A.

Like for most horns, the corrugations of our reference horn are $\lambda/4$ in width and depth in the main conical region. In the matching section, the width changes and the depth increases from $\lambda/4$ to $\lambda/2$ at the beginning of the throat. All three helicoidal horn corrugations have been designed with the same width and depth, but this time the width is $\lambda/4$ everywhere including in the matching section. The reference horn's waveguide flange is in WR-10, with the circular-to-rectangular waveguide transition integrated within it. It is followed by a commercial WR-10-to-WR-8 transition. In the case of A, B, and C, the horns have a circular waveguide flange, and the circular-to-WR-8 transition is achieved by means of an external transition.

One potential difficulty with the helicoidal design resided in the broken symmetry. From one fabricated horn to the next, the threads could start and end at any angular position within the (x,y) plane of the matching section and of the aperture. We assumed that this uncontrolled assymmetry would likely reflect on the measured beam pattern and cross-polarization of the horn. Consequently we decided to accurately control the angle α made by the threads with the waveguide E field polarization, as shown in Fig. 3, and to systematically study its effect on horn performance. To do this, we have inserted a custom-made circular waveguide rotating adapter [5] between the horn's circular waveguide flange and the WR-8 rectangular-to-circular waveguide transition, to play at will with the parameter α (see Fig. 3). Since the surface currents and the field are much larger in the mode-launching section than in the aperture plane, we expected the role of threads in the throat to be dominant and we have thus concentrated our study to this region. Note, however, that by playing very slightly with the length of the horn one could also independently study potential effects of the treads position in the aperture plane.

Table 1 summarizes the physical dimensions of the reference and helicoidal horns used in our 100-120 GHz measurements. The three corresponding aluminum mandrels [6] are shown in Fig. 4.

Feedhorn	Reference	A	B	C
Number of threads	0	1	2	3
Material	copper	'Roses' alloy	'Roses' alloy	'Roses' alloy
Aperture diameter [1]	13.35	13.35	10.12 [2]	13.35
Semi-flare angle	8°	8°	8°	8°
Total Length	38.32	38.0	25.0 [2]	38.0
Throat length	8.02	8.0	8.0	8.0
Circular waveguide Diameter, Length	2.56 6.78	2.36 5.0	2.36 5.0	2.36 5.0
Rotating adaptor length	none 0	yes 20.0	yes 20.0	yes 20.0
Circular-Rectangular Transition length	19.3	30.0	30.0	30.0
Rectangular waveguide a x b	WR-10 2.54 x 1.27	WR-8 2.12 x 1.06	WR-8 2.12 x 1.06	WR-8 2.12 x 1.06
Corrugations : Width Depth	 0.45 0.7	 0.45 0.7	 0.45 0.7	 0.45 0.7
Start of throat : Width Depth	 0.45 1.4	 0.45 1.4	 0.45 1.4	 0.45 1.4

[1] All dimensions in mm.

[2] Horn B was amputated of 13 mm from the aperture because of a molding defect.

Table 1. Summary of thysical dimensions of the 'reference' classically corrugated horn and of the single thread, double thread and
triple thread helicoidal horns.

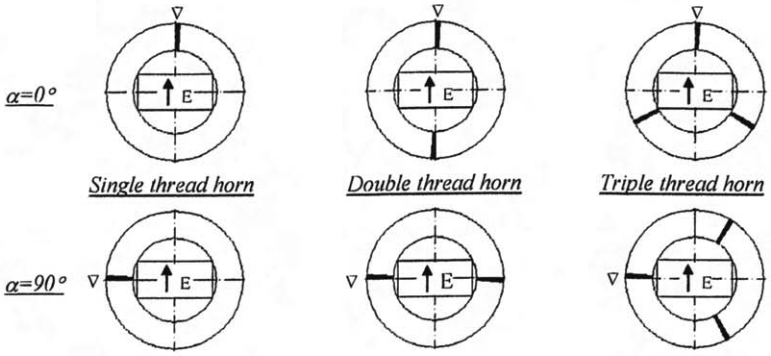

Fig. 3. Thread orientation with respect to the waveguide E field, defined by the angle α. The influence of α was studied for the single, double and triple thread 110 GHz horn prototypes. Configurations having the thread(s) aligned with the E field were set to α=0°.

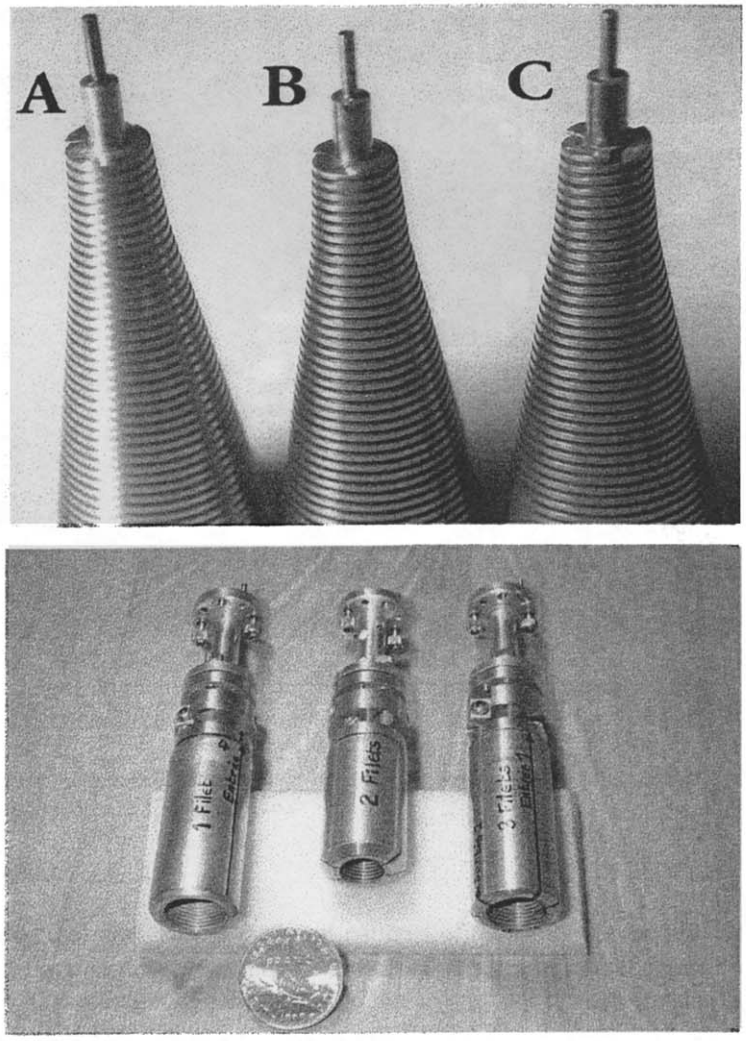

Fig. 4. (a) Photograph of the three helicoidal aluminum mandrels designed for 110 GHz with one, two and three threads ; (b) Photograph of the fabricated helicoidal horns mounted to their rotating circular waveguide adapters.

3.2. Measurement setup.

The measurements were performed from 100 GHz to 122 GHz using an ABmm millimeter vector network analyzer [7]. The emitter was a 110 GHz corrugated horn, identical to the reference horn, fed by a Gunn oscillator source. The receiver was the horn under test, connected to a lab-made Schottky harmonic mixer and mounted on a precision rotating plate moved by a computer-controlled stepper motor. The distance between the source and the horn under test was set to more than 16 D^2/λ, where D is the aperture of both emitter and receiver horns and λ the free space wavelength. In this configuration the dynamics available on the ABmm was about 80 dB. Great care was taken to avoid spurious reflections off walls and waveguide parts, using absorbing material [8]. The complete setup is shown in Fig. 5.

The cross-polar radiation was measured with a dynamic range of 50 dB. This was achieved using a grid polarizer inserted in the optical path in front of the emitter, so as to avoid measuring a combination of the cross-polarization characteristics of both the emitter and the horn under test. This grid was mounted on a precision rotation mount and surrounded by RF absorbers to avoid leakage.

For every horn, the phase center of the horn under test was found by iterative adjustments of its position relative to the θ–rotation axis either in the z direction or laterally. Also, these measurements were made for many angles α sampled between 0 and 360°, by steps of 15°, by revolving the feedhorn about its geometrical axis using

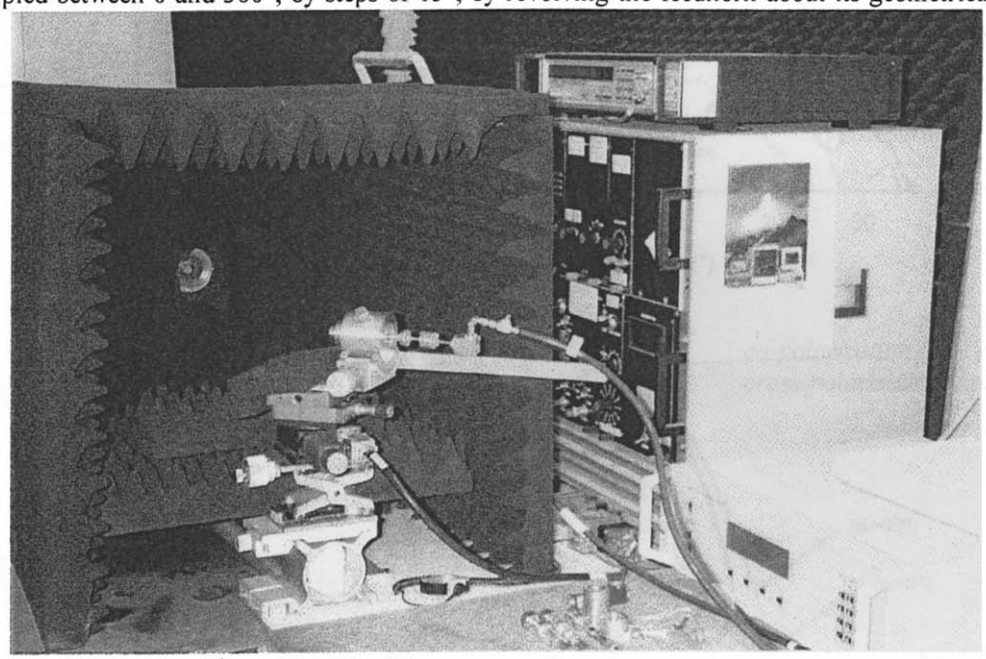

the circular waveguide rotating adapter.

S_{11} parameter measurements were done with the same bench. Instead of facing the emitter, the horns under test were set up in the beam pattern measurement test bench to load them with a perfect absorber.

Fig. 5. Test bench with the ABmm millimeter vector network analyzer used for S11, co-polar, cross-polar amplitude and phase and measurements from 100 GHz to 122 GHz.

3.3. Beam measurements.

Figure 6 shows the co-polar and cross-polar beam patterns of the single-thread horn 'A' measured at 110 GHz in the E and H planes, for two angles α = 0° and α = 90°. The patterns of the reference horn, measured with the same setup, are also shown. We note a very good overlay of the main lobes of the helicoidal horn and the reference, both in the E and H planes. The near Gaussicity of the horn can be seen in Fig.7, where the measured amplitudes and phases at α=90° in both planes are superimposed. Yet this is specific to a certain thread angle, and with α=0° the symmetry between the E and H-plane is lost. At 110 GHz, the single thread horn presented low side lobe levels (below –23 dB) in both E and H-plane and with the two positions of the thread (α=0° and α=90°). This conclusion remains true for intermediate values of α, as seen in Fig. 9.a.

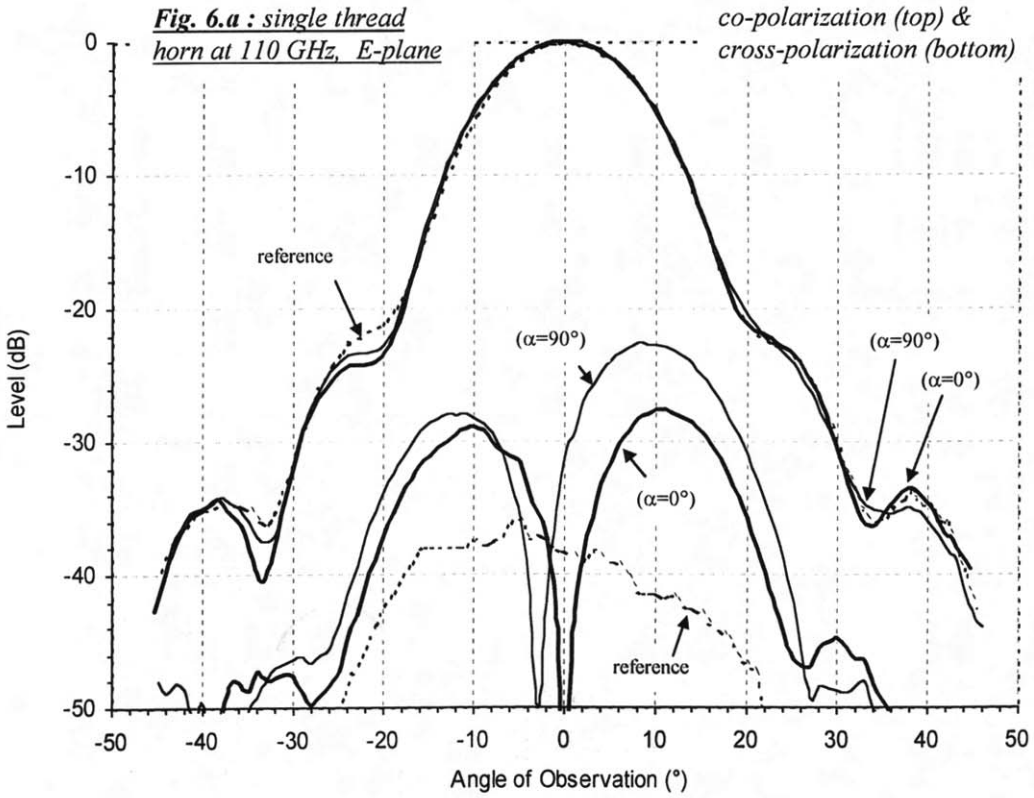
Fig. 6.a : single thread horn at 110 GHz, E-plane
co-polarization (top) & cross-polarization (bottom)
reference
(α=90°)
(α=90°)
(α=0°)
(α=0°)
reference
Level (dB)
Angle of Observation (°)

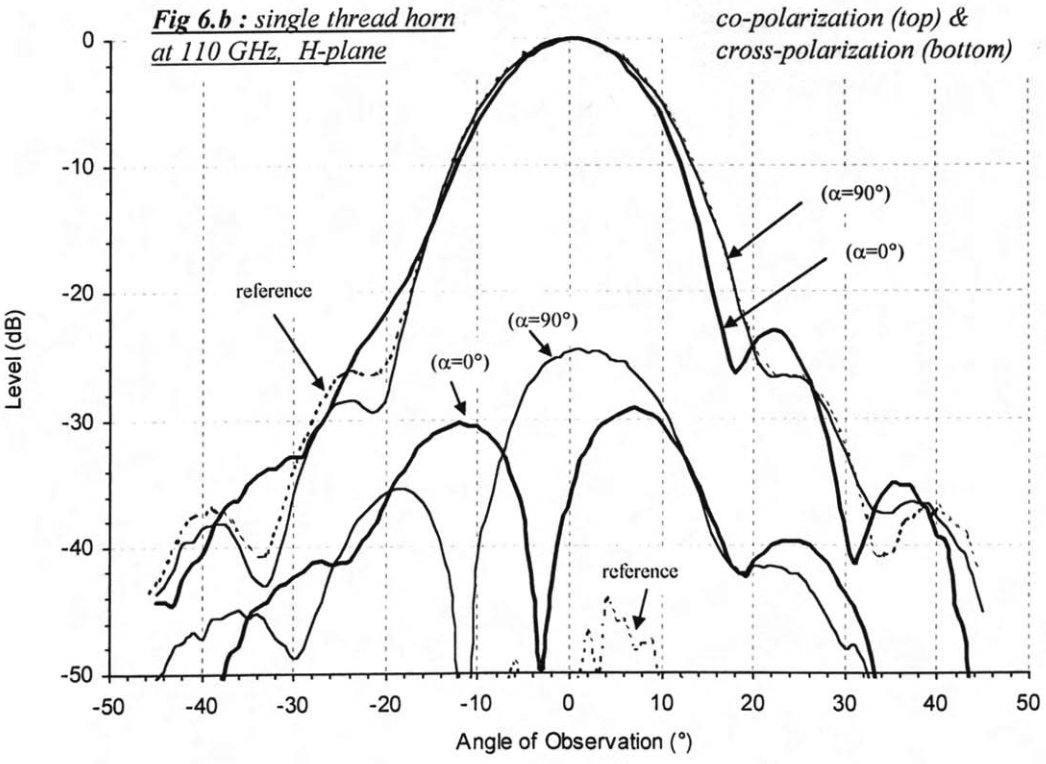
Fig 6.b : single thread horn at 110 GHz, H-plane
co-polarization (top) & cross-polarization (bottom)
(α=90°)
(α=0°)
reference
(α=90°)
(α=0°)
reference
Level (dB)
Angle of Observation (°)

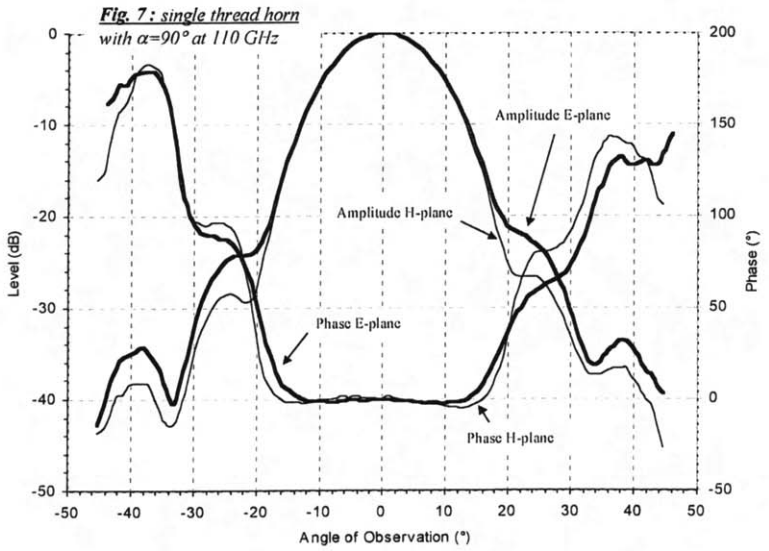

Fig. 7 : *single thread horn with α=90° at 110 GHz*

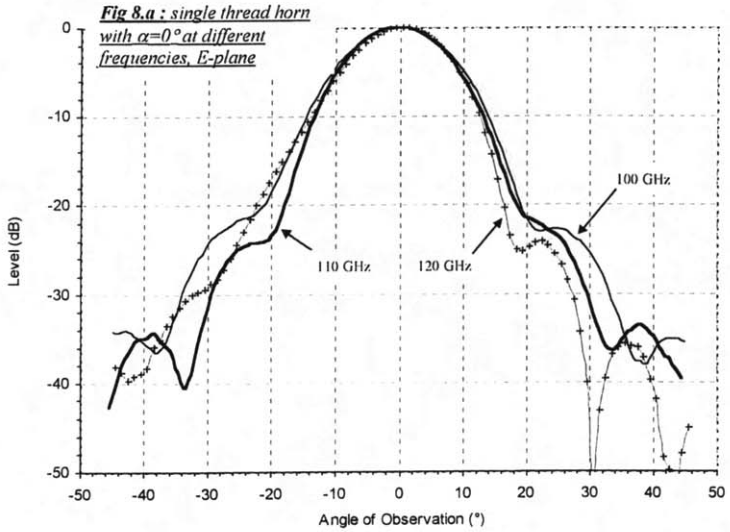

Fig 8.a : *single thread horn with α=0° at different frequencies, E-plane*

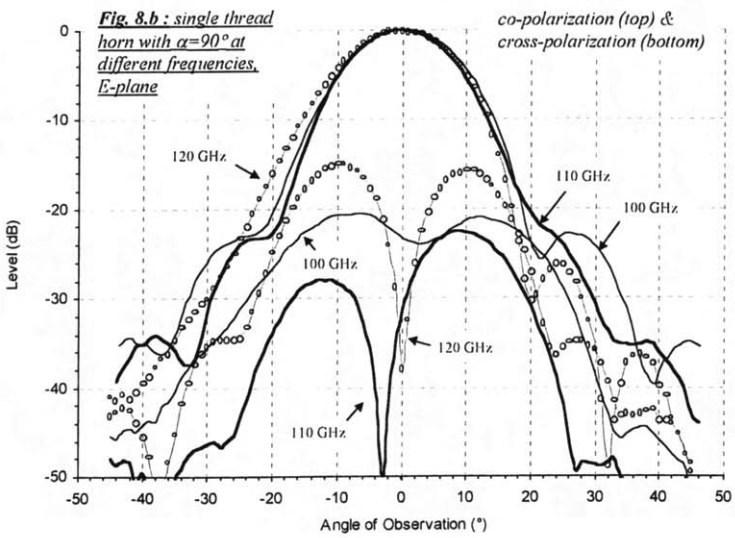

Fig. 8.b : *single thread horn with α=90° at different frequencies, E-plane*

co-polarization (top) & cross-polarization (bottom)

However, some very unique assymmetry is seen with the helicoidal horns. Certain sidelobes tend to become 'shoulders' smoothly departing from the main lobe. This situation somewhat blurs our common definition of a sidelobe. On the curves one can both see clearcut sidelobes with a well defined nul in the diffraction pattern, and vague shoulders fattening the main lobe on one side at the -20 dB level. From this point of view, the H plane seems much more sensitive than the E plane to varying values of α. Interestingly, in either measurement plane, one observes an exchange between one side of the main lobe and the other, as to where the sidelobe and the shoulder appear. This assymmetry varies not only with α but also with frequency (figs. 8.a and 8.b). How the beam pattern asymmetry varies with frequency seems to be independent of α. One should not dismiss the possibility of some small level of axial misalignment between the mandrel and the horn during fabrication, which could explain the slight precession observed in Fig. 9.a.

As one could intuitively expect, the double thread horn 'B' possesses the most symmetric beam of all three horns (Fig. 10). At 110 GHz, for both positions of the threads α=0° and α=90°, the double thread horn shows a perfect E-H plane symmetry for levels higher than –18 dB (Fig. 11). Below this level, an asymmetry in the E and H planes is seen, although the beam pattern itself stays symmetrical. As seen in Fig. 9.b, α still plays a role in the sidelobe level, but less than for 'A' and without ever destroying the beam symmetry. Also, no angular deviation of the main lobe with α is noted as in the single-thread horn, which might indicate some kind of axial misalignment. At α=0° the sidelobes are accurately defined and at their lowest level, below - 26 dB.

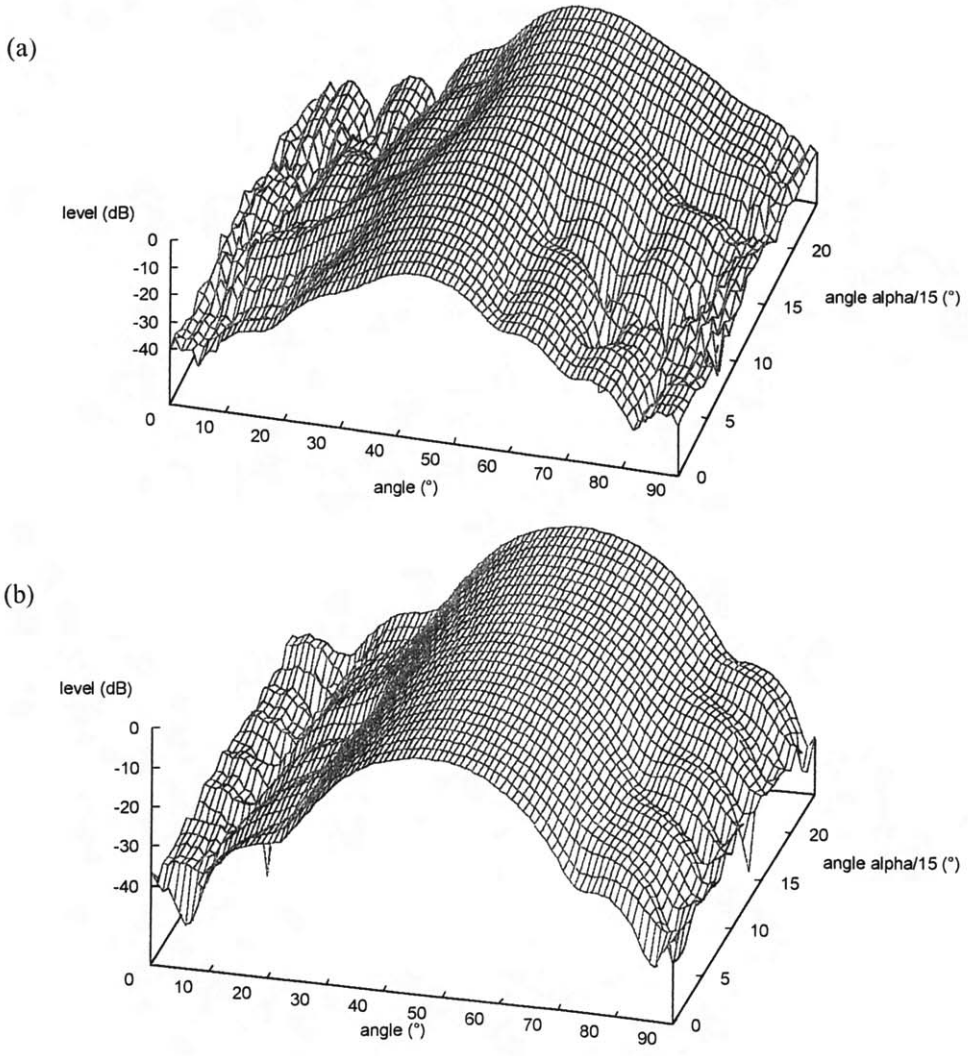

Fig. 9. Co-polar beam pattern versus α for the (a) single thread and (b) double thread horns. Increments are 15° steps.

We note that the main lobe is wider than for the reference and the other helicoidal horns. This is only due to 'B' being physically shorter than its 'A' and 'C' counterparts (see Table 1). It was deliberately truncated as a result of a manufacturing defect near the aperture. The performances were found to be as good at 120 GHz as at 110 GHz, for the positions of the threads $\alpha=0°$ and $\alpha=90°$ (Fig. 12).

At 110 GHz, the triple thread helicoidal horn presents a main lobe similar to that of the reference and low side lobes levels (Fig. 13.a and 13.b). Qualitatively, the triple thread horn 'C' looks more like 'A' than 'B', having more beam pattern asymmetry. The best case with respect to symmetry seems to be for $\alpha=0°$, in both planes E and H. The dependance on frequency (Fig. 14) and α of the beam asymmetry is similar to what has already been observed in the single-thread case, but one only sees 'shoulders' and no true sidelobes anymore beside the main lobe. When increasing the frequency to 120 GHz, the beam pattern is almost unchanged.

One can understand this as an averaging effect. When the number of threads is increased, a smaller rotation angle α is needed to fall back on the exact same thread configuration. Put differently, increasing the number of threads will end up restoring the beam symmetry.

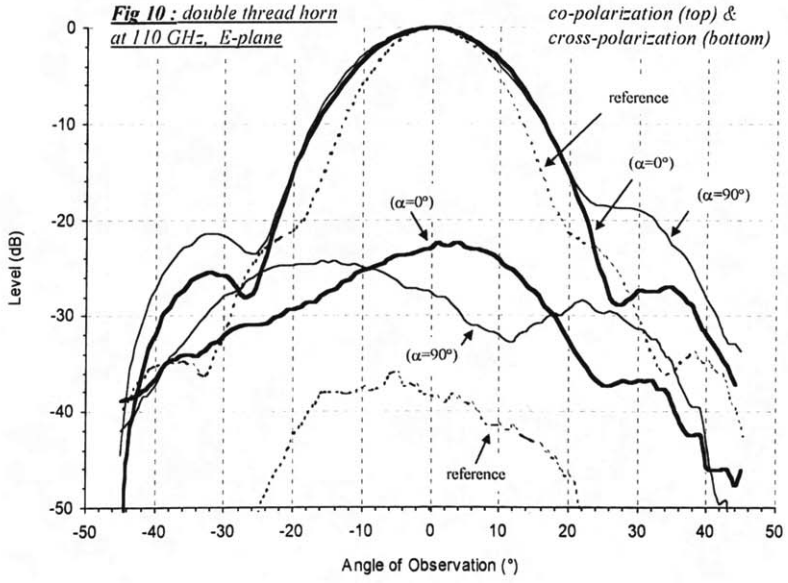

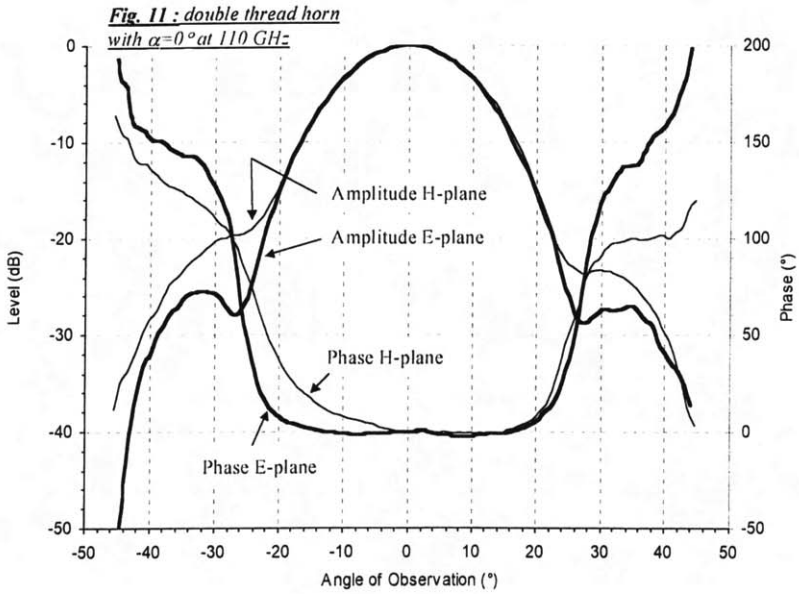

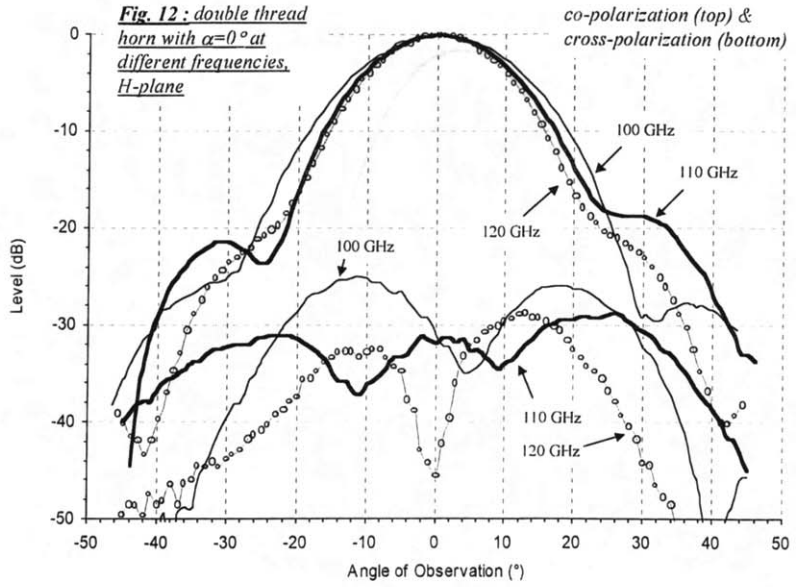

Fig. 12 : *double thread horn with α=0° at different frequencies, H-plane*

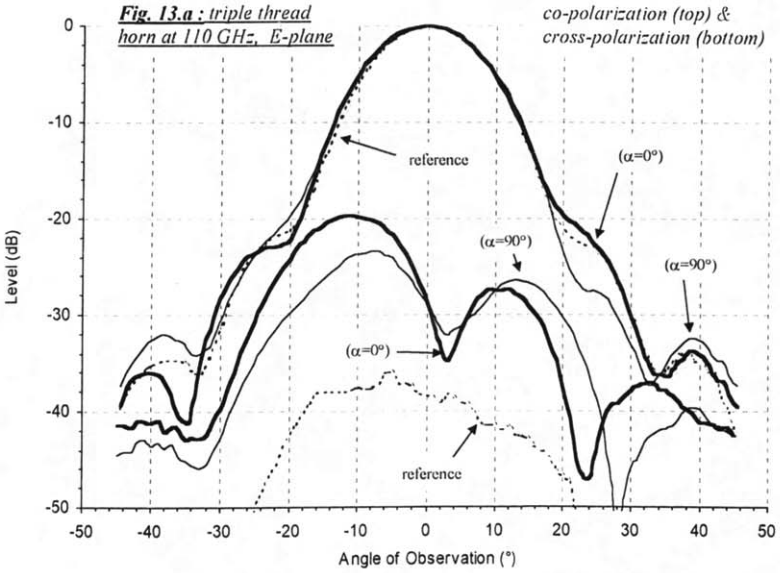

Fig. 13.a : *triple thread horn at 110 GHz, E-plane*

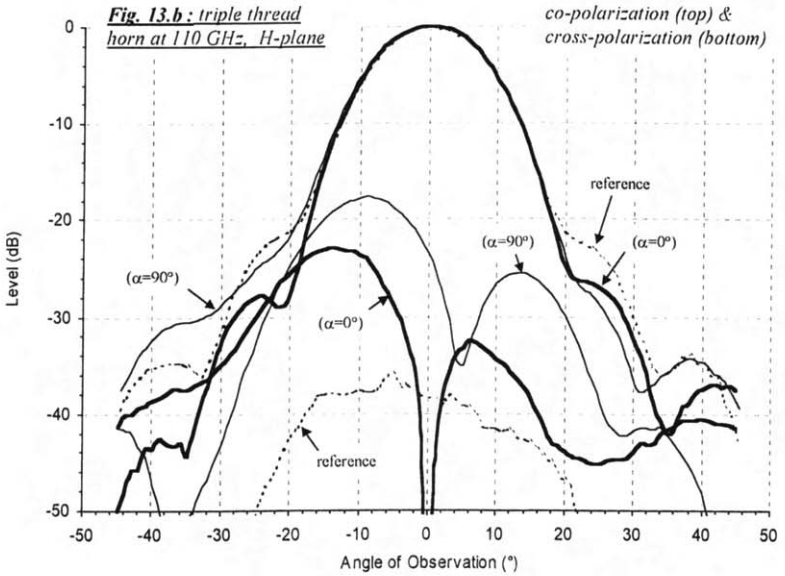

Fig. 13.b : *triple thread horn at 110 GHz, H-plane*

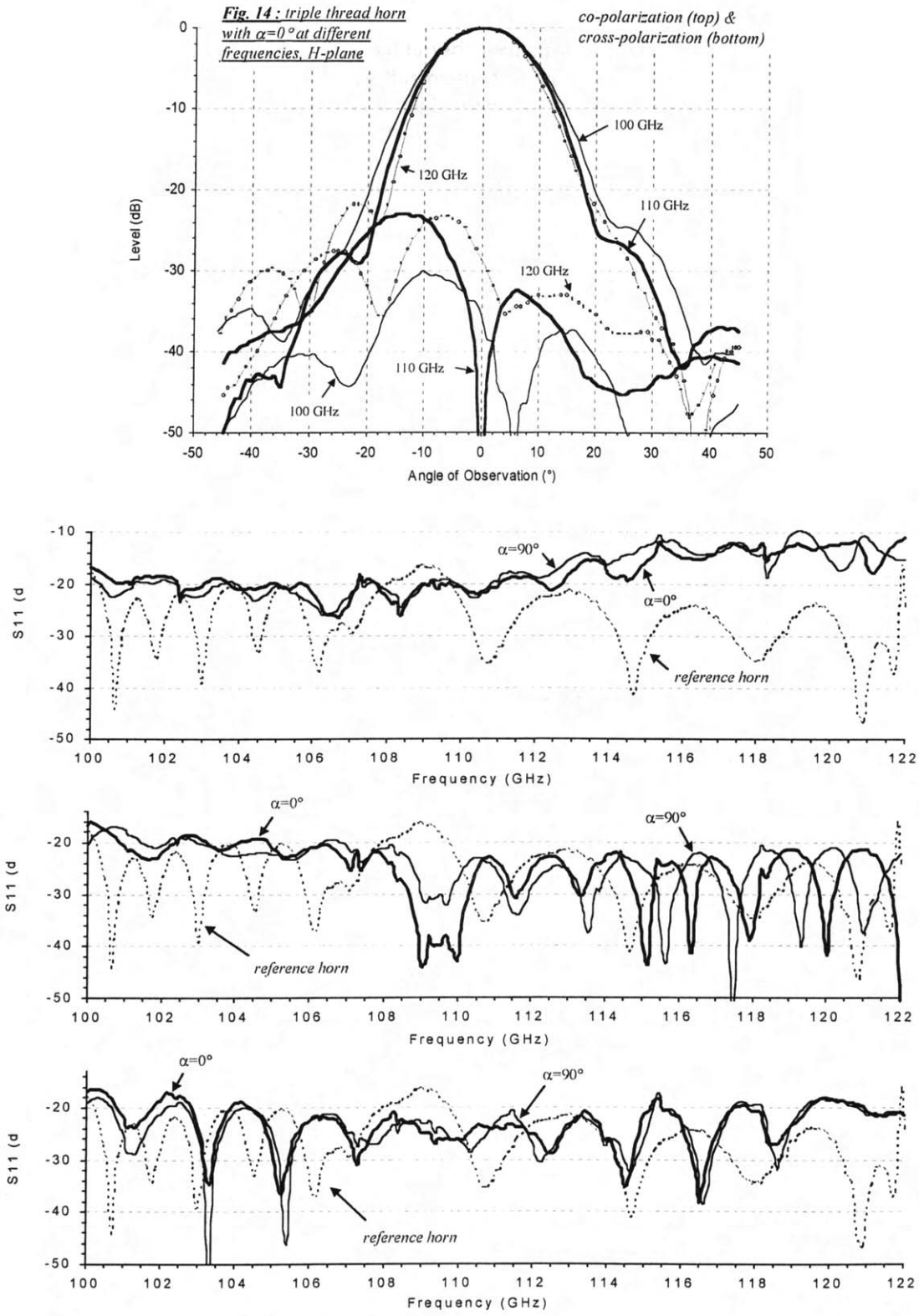

Fig. 15. Measured S_{11} for the single (top), double (middle) and triple (bottom) thread horns. The reference is also shown.

3.3. Cross-polarization measurements

The single thread horn shows good to very good cross-polarization levels at 110 GHz (Fig. 6.a and 6.b). Best results were found when α=0°; with this position of the thread, the cross-polarization is as low as –30 dB. Nevertheless, the performances decreases strongly when the frequency reaches 120 GHz (Fig. 8.b). Levels of about –15 dB to –13 dB were measured at 120 GHz with α=0° and α=90° respectively.

The double thread horn showed good and relatively observation-angle-independent cross-polarization levels (Fig. 10). Maximum levels of –25 dB to –23 dB were found. The two positions of the threads appeared to be quasi equivalent in terms of performances (off the horn-axis, while α=0° was a better position than α=90° in the E-plane, the situation was the opposite in the H-plane). In the H-plane and at 110 GHz, the levels are below –30 dB (Fig. 12). Unlike the single thread horn, the double thread horn has slightly better cross-polar levels at higher frequencies (-30 dB to –25 dB at 120 GHz).

The triple thread horn presents average to good cross-polarization levels. Levels below –20 dB are measured in the E-plane (Fig. 13.a) and below –18 dB in the H-plane (Fig. 13.b). At 120 GHz, the cross-polarization levels are the same. We found that α=0° is a position of the thread a little better than α=90°. Nevertheless, the difference between both positions is much smaller with the triple thread horn than with the single thread horn.

3.4. S_{11} parameter measurements

The measurements showed an acceptable to very good matching over a 20% bandwidth, for all helicoidal horns (Fig. 15). The double thread helicoidal horn gave the best performances, with S_{11} between -23 dB to -20 dB through the whole band. Its performance is comparable to the reference horn, if not better. We noticed that the matching was nearly the same for either of the positions of the threads that we chose, except for the double-thread horn, which has a plateau at -40 dB (α=0°) or -30 dB (α=90°) at 110 GHz.

4. DISCUSSION

Several results pertaining to the introduction of a helicoidal shape should be stressed out. In particular, we have found the location of the thread starts in the throat relative to the waveguide to have a strong influence on both the co-polar and cross-polar radiation patterns. This is no surprise, since it reflects a geometrical asymmetry of the aperture. It implies one must carefully study how a particular helicoidal geometry, be it by the number of threads or the angle α, should be chosen. Indeed, we find that certain horns, described by a certain number of threads and a certain angle α, behave more nicely than others, as far as beam pattern symmetry, cross-polar level and VSWR are concerned.

For all three types of helicoidal horns, maximum cross-polar radiation levels were found to be less than -20 dB. For other values of angles α and θ, it drops to very small levels, similar to what the reference horn gives (-40 to -50 dB). This seems acceptable for most applications. It also seems that all horns perform more or less similarly, despite the influence of the number of threads and of the angle α. Cross-polarization may not be a severely driving criterion to select one particular type of horn.

The fact that cross-polar levels peak to higher values than in the classical horn case could be due to some rotation of the field in the dominant spherical hybrid HE_{11} mode. But it is also suggestive of mode conversion occuring within the horn. This mechanism could be more important in helicoidal horns than in circular corrugated horns since higher order modes could be specifically triggered by the threads in the mode-launching section. We observe that the variation of cross-polar level versus frequency is qualitatively quite different from what is seen for the classical horn. In addition, what is measured clearly depends on the numbers of threads (1, 2 or 3) and on α. These facts strongly point to a mode conversion induced by the threads. This hypothesis can be tested by simulations using, for example, a spherical wave expansion method.

For A, B and C, the measured S_{11} parameter was always higher than that found for the reference horn. This was to be expected since on the helicoidal horns the matching could not be optimized with a varying width-to-pitch ratio in the throat. Nevertheless, the S_{11} values obtained are probably good enough for many applications. We should note that the single-thread horn is worst than the others while the double-thread helicoidal horn gives the lowest return, below 20 dB over the whole 20% bandwidth, with a nice plateau around the center frequency at -40 dB (α=0°) or - 30 dB (α=90°).

From the point of co-polar beam pattern, the double-thread horn 'B' with $\alpha=0°$ is the most symmetrical, with very low sidelobes at -26 dB, that is, better than the reference horn. Its larger main lobe is only due to the smaller aperture, since 'B' had to be truncated. Also, the cross-polar radiation is flatter versus observation angle θ than for A and B. These observations, together with the low return loss, designate the double-thread, $\alpha=0°$, helicoidal horn as the best candidate so far. It is worth noting that $\alpha=0°$ corresponds to placing the thread starts at both positions where the intensity of microwave currents in the waveguide is zero.

Although the tests have been done for 110 GHz prototypes, there is no frequency limitation to the helicoidal technique other than the usual difficulty to machine increasingly small mandrels. On the contrary, it may be easier to accurately replicate small corrugations through molding rather than through electroforming. Since our process is done under alloy pressure and under vacuum, the filling efficiency is quite large and there is no such thing as voids in the horn filled with caustic electrolyte solution, a problem often encountered with electrodeposition processes for small corrugations. For even smaller corrugations (above 1 THz), an adaptation of the molding process will be reported elsewhere. Figure 16 shows single-thread helicoidal mandrels machined for 1 THz [9].

The cost reduction obtained with this technique is evident and two-fold. The mandrels represent one expensive part of the electroforming process, especially at submillimeter wavelengths where corrugations are hard to machine. Instead of making one mandrel for each horn, with the technique proposed here only one or two mandrels will suffice to produce a nearly unlimited number of identical horns. On the other hand, the long time necessary to electroform many horns has also a large cost. This cost is dramatically cut back by switching to the new technique.

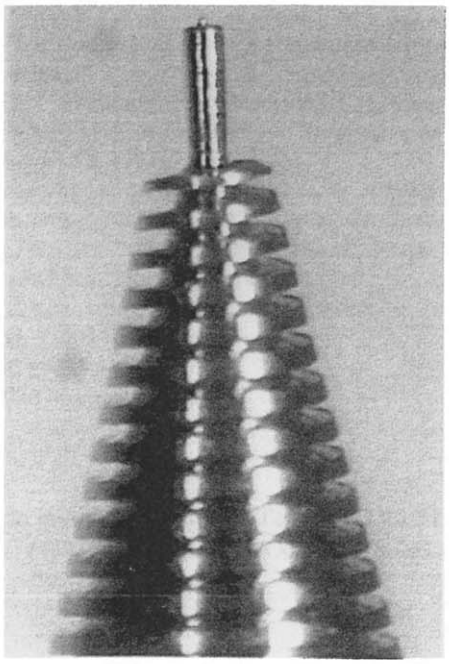

Fig. 16. Photograph of a 1 THz helicoidal mandrel, machined out of titanium.

5. CONCLUSION

We propose a new technique for manufacturing low-cost corrugated feedhorns. This new process is based on molding horns after a single master aluminum mandrel with helicoidal thread corrugations. Such a mandrel can be 'unscrewed' and reused many times, instead of being etched away as in the current electroforming process. We have fabricated and characterized at 100 GHz helicoidal horns with one, two and three threads, based on the design of a classical reference horn. As a consequence of the replacement of usual concentric corrugations by a helicoidal thread, some asymmetry can be observed in the beam patterns, reflecting the broken corrugation symmetry. In addition, helicoidal horns show a somewhat higher cross-polarization levels than classical corrugated horns. Nevertheless, these effects are all under -20 dB. Furthermore, we have noticed a significant improvement when

using a double thread, which has a perfectly symmetric beam pattern with sidelobes at -26 dB (better than the reference horn) when the thread start is aligned with the waveguide field polarization. The double-thread horn also shows the smallest VSWR over the 20 % measurement bandwidth. Further study will focus on the theoretical modeling of these horns in order to optimize the mode-launching section and control the beam pattern asymmetries. These new types of horns can probably compete with the classical corrugated horn in terms of matching, beam pattern and cross-polarization level, for many microwave remote sensing and telecommunication applications, and particularly for X-band, millimeter-wave and supra-THz frequencies. Because numerous identical horns can now be cost-effectively fabricated after a single master mandrel, this technique is very well suited to multi-pixel waveguide receivers, radiometer arrays (e.g. ALMA), or any other application for which mass production of feeds is needed.

ACKNOWLEDGEMENTS

This work has been funded by the Centre National de la Recherche Scientifique, patent pending CNRS # 9800271, and by the French Ministère de l'Education Nationale, de la Recherche et de la Technologie, via Paris Observatory's *Bonus Quality Research* scientific budget. We are indebted to P. Goy of ABmm for his invaluable help in relation to the vector network analyzer measurements. We warmly thank M. Gheudin for numerous and helpful technical discussions, J.-P. Ayache and Paris Observatory mechanical department for their technical assistance. We also acknowledge G. Beaudin and Y. Viala for their encouragement and support.

REFERENCES

1. P.J.B. Clarricoats and A.D. Olver, *Corrugated Horns for Microwave Antennas*, IEE Electromagnetic Wave Series 18, Peter Peregrinus Ltd, London, 1984.
2. B.N. Ellison, M.L. Oldfield, D.N. Matheson, B.J. Maddison, C.M. Mann and A.F. Smith, 'Corrugated feedhorns at Terahertz Frequencies', *Proceedings of Fifth International Symposium on Space Terahertz Technology*, pp. 851-860, U. of Michigan, Ann Arbor, May 10-12, 1994.
3. B. M. Thomas, 'Design of corrugated conical horns', *IEEE Trans. Antenna Propagat.*, **vol. AP-26**, pp. 367-372, 1978.
4. Mandrel made by Meudon Observatory's *Service d'Etudes et Réalisations Techniques* ; Electroforming and Gold-Plating done by *Protection des Métaux*, 57-59 rue de Saint-Mandé, 93100 Montreuil, France.
5. *S.A. Musy*, 12 rue des grattes, 1337 Vallorbe, Switzerland.
6. *Société Audoise de Précision*, Z.A. du Pont, 81500 Ambres, France.
7. *AB Millimètre,* 52 rue Lhomond, 75005 Paris, France.
8. *Emerson & Cuming,* Eccosorb® CV3, unpainted.
9. *MASSIP*, 4 rue des frelons, 77720 Mormant, France.

---

* Correspondance : Email : jean-marie.munier@obspm.fr ; Tel : (33)1.40.51.22.56 ; FAX : (33) 1.40.51.20.85 ; alain.e.maestrini@jpl.nasa.gov ; Tel : (1)818.354.58.92 ; FAX : (1)818.393.46.83.